

EVALUATION OF TRM IN THE COMPLEX THROUGH WALL ENVIRONMENT

W.-J. Zheng, Z.-Q. Zhao, Z.-P. Nie, and Q.-H. Liu [†]

School of Electronic Engineering
University of Electronic Science and Technology of China
Chengdu, Sichuan 610054, P. R. China

Abstract—Practical interests arising from behind-the-wall target detection, surveillance and reconnaissance et al. claim for high capability of imaging in complicated environments. Time Reversal Mirror (TRM) technique, making use of the principle of reciprocity, emerges as a promising way to deal with such complex problem. In this paper, we investigate TRM in the ultra-wideband (UWB) through wall radar imaging (TWRI) through numerical simulation. The probing region is a square room, with walls of rough surface and random media parameters. TRM is used to image the target settled in the room. We evaluate the degradation of the images when the aperture of the array is decreased or the received signals are contaminated by noises. The back projection (BP) algorithm is employed here as a comparison for imaging quality. For the case in which the random walls are changed between the forward and inverse phase of time reversal, we check the imaging stability and applied an averaged Green's function to improve the imaging quality. Finally, some interesting conclusions are drawn.

1. INTRODUCTION

In the through wall radar imaging (TWRI), relatively high-density materials like concrete and bricks can result in considerable attenuation of electromagnetic waves and cause the multi-path propagation of the signal. This increases the requirements for both radar power and signal processing. Conventional narrow-band systems are no longer applicable here due to their poor down-range resolution. In contrast, UWB radar which can produce higher resolution and power efficiency

Corresponding author: Z. Q. Zhao (zqzhao@uestc.edu.cn).

[†] The last author is also with Department of Electrical and Computer Engineering, Duke University, Durham, NC 27708, USA.

is the most promising candidate. Several papers [1–4] have reported the applications of UWB technique to TWR. And some UWB TWR systems have been built [5–8].

Concerning the imaging processing in TWR, several effective imaging algorithms (e.g., [9–13]) have been proposed and discussed. [9] developed an 2D contrast source inversion (CSI)-based imaging technique in a layered medium to model the effects of the building walls. [10] introduced the back projection imaging algorithm to the stepped-frequency TWR. In [13], based on higher order statistics, the author presented an autofocusing technique to correct for errors under unknown walls. However, in the heterogeneous and highly scattering environment, although the back-scattered signal level may be sufficiently above the noise level, signal between target and radar may experience many reflections and diffractions. Therefore, many imaging methods may need complex process to minimize multipath effects, i.e., to compensate the effects of the walls, such as refraction, attenuation, et al.

TRM, which has been demonstrated both theoretically and experimentally in an extensive set of ultrasonic and acoustic literatures [14–20], as well as in recent electromagnetic studies [21–28], is widely regarded as a powerful tool for imaging, especially in the complex environment. [29] reported a preliminary application of TRM in UWB-TWRI. In this paper, more actual environment is taken into consideration. The probing region is a square room. The walls are randomized with rough surface. FDTD algorithm is employed to simulate the electromagnetic wave propagation. We evaluate the imaging capacities of TRM in such random setting. At the condition which the size of the transmitter-receiver array is decreased or the space between two adjacent transmitters is enlarged, we assess these impacts on the images. For actual consideration, some blurring of the recorded data should be modeled. We artificially add some noises in the received signals and investigate TRM imaging with these contaminated signals. The back projection (BP) algorithm is employed here as a comparison for the imaging quality. For the case in which the random walls are mismatched between the forward and inverse phase of time reversal, we check the imaging stability and applied an averaged Green's function to improve the imaging quality.

This paper is organized as follows: in Sec. 2 the main principles of TRM technique in TWRI are provided. In Sec. 3, several issues concerning TRM in UWB-TWRI are proposed and discussed. Model description is given in Part 3.1. TRM is performed to image a target settled in the room in Part 3.2. In Part 3.3, we study TRM with the contaminated signals. Some imaging results for using TRM are

compared with that of using the BP imaging algorithm. In Part 3.4, we investigate the impact of a narrow array for TRM in TWRI. And in Part 3.5, we check TRM in the mismatched environment and apply an averaged Green's function to improve the image quality. Some useful conclusions are drawn in the last section.

2. TIME REVERSAL MIRROR (TRM) TECHNIQUE

TRM is a technique which is based on the principle of reciprocity. Its basic principle can be described as following. Assume a source emits radiation that propagates through the complex media with the time-domain fields measured by an array of receivers. The recorded signals are time reversed in the time domain (or phase conjugated in

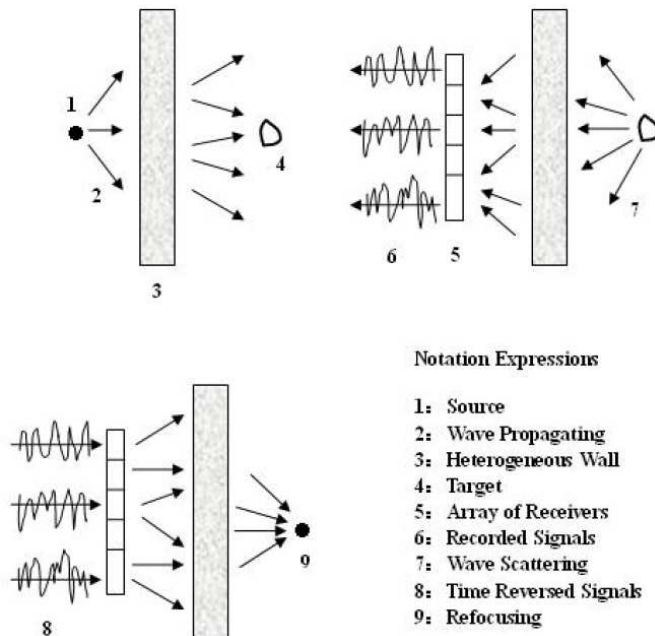


Figure 1. Basic procedure of TRM in the TWRI. Top left: A source emits radiations that penetrate through the heterogeneous wall, illuminate the target in the other side of the wall. Top right: Fields are reflected back, recorded by a linear array which is located behind the original source. Bottom left: Signals are time reversed in the time domain, re-emitted; recreate the tighter refocusing in the target's location.

the Fourier domain), re-emitted from their respective reception points. Due to the time reversibility of the wave equation in the non-absorbing media, all of the energy arrives at the original source in unison, approximately recreating the original excitation. The transmitter-receiver array has been termed as time-reversal mirror (TRM) [14].

In the TWRI, the locations of the targets need not be known. Targets reflections are employed as second sources illuminate the array of receivers in echo mode (as depicted in Fig. 1). By computational time reversing, the back-propagated fields focus near the active targets. General mathematical descriptions of its basic principle in TWRI are given as followings (For simplicity, we just use scalar fields here).

Assuming a short time domain pulse $p(t)$ emitted from a transmitter which is located at \mathbf{r}_S , field propagates through the time-invariant heterogeneous media, illuminates the targets situated at \mathbf{r}_m , $m = 1, 2, \dots, M$. The incident field observed at \mathbf{r}_m due to the original source is

$$U_F(\mathbf{r}_m, \omega) = \hat{p}(\omega) \hat{G}_F(\mathbf{r}_m, \mathbf{r}_S, \omega) \quad (1)$$

where the Fourier transform of the pulse is

$$\hat{p}(\omega) = \frac{1}{2\pi} \int_{-\infty}^{\infty} p(t) e^{i\omega t} dt \quad (2)$$

The Green's function $\hat{G}_F(\mathbf{r}_m, \mathbf{r}_S, \omega)$ satisfies the reduced wave equation

$$\nabla^2 \hat{G}_F(\mathbf{r}, \mathbf{r}_S, \omega) + \varepsilon(\mathbf{r}) \mu(\mathbf{r}) \omega^2 \hat{G}_F(\mathbf{r}, \mathbf{r}_S, \omega) = -\delta(\mathbf{r} - \mathbf{r}_S) \quad (3)$$

where $\varepsilon(\mathbf{r})$ is the dielectric constant, $\mu(\mathbf{r})$ is the magnetic permeability.

The M targets reflect the fields, act as M positive sources. The equivalent scattered fields that converted from the incident fields $U_F(\mathbf{r}_m, \omega)$ are

$$U_R(\mathbf{r}_m, \omega) \approx c_m(\omega) U_F(\mathbf{r}_m, \omega) \quad (4)$$

where $c_m(\omega)$, $m = 1, 2, \dots, M$ is the complex frequency-dependent reflectivity coefficients.

The fields radiate back, illuminate a linear array with K elements (receivers). Signals are recorded for a long enough time T to avoid missing the multiple reflected fields. On the k th element the recorded signal is

$$u_T(\mathbf{r}_k, t) = \sum_{m=1}^M \int_{-\infty}^{\infty} U_R(\mathbf{r}_m, \omega) \hat{G}_F(\mathbf{r}_k, \mathbf{r}_m, \omega) e^{-i\omega t} d\omega \quad (5)$$

In the through wall application, the background information (such as the approximate dielectric constant and the thickness of the

wall) may be roughly estimated. The background signature can be measured as $u_G(\mathbf{r}_k, t)$ a priori. Therefore, the target signature can be obtained approximately by subtracting the background signature from the signature with the target in the background. So in the frequency domain, we have

$$U_B(\mathbf{r}_k, \omega) = \frac{1}{2\pi} \int_{-\infty}^{\infty} \chi(\mathbf{r}_k)(u_T(\mathbf{r}_k, t) - u_G(\mathbf{r}_k, t))e^{i\omega t} dt \quad (6)$$

Signals are time reversed in the time domain (conjugated in the Fourier domain) and re-emitted from the respective reception positions. The space-time signal observed at the imaging domain is

$$I(\mathbf{r}, t) = \sum_{k=1}^K \int_{-\infty}^{\infty} U_B(\mathbf{r}_k, \omega)^* \widehat{G}_C(\mathbf{r}, \mathbf{r}_k, \omega) e^{-i\omega t} d\omega \quad (7)$$

which in the Fourier domain is

$$\widehat{I}(\mathbf{r}, \omega) = \sum_{k=1}^K U_B(\mathbf{r}_k, \omega)^* \widehat{G}_C(\mathbf{r}, \mathbf{r}_k, \omega) \quad (8)$$

where $G_C(\mathbf{r}, \mathbf{r}_k, \omega)$ represents the computational Green's function from the k th element to the imaging domain. The symbol “*” denotes complex conjugation.

Usually, according to the imaging principle, the focusing quality (resolution) is determined by the size of the array aperture. In a homogeneous medium, the computational Green's function equals to the actual one, the cross range resolution (in directions parallel to the array) is $\lambda L/a$ and the range resolution is $\lambda(L/a)^2$ [30] (a is the physical aperture, L is the propagation distance, λ is the carrier wavelength of the probing pulses). In a heterogeneous, multipathing environment, TRM technique can achieve much better resolution [15, 31]. This phenomenon is called super-resolution and comes from multipath caused by the media heterogeneities. Theoretically analysis in [31] provided an effective aperture formula for a finite aperture or Gaussian TRM in random media

$$a_e(L) = a \sqrt{1 + \frac{L^3 \gamma}{a^2}} \quad (9)$$

where γ is a constant with respect to the randomness of media parameters. For a pulse in the time domain, super-resolution is linked to the effective aperture a_e of the TRM.

Moreover, experimental studies in [15, 32] show a remarkable stability of the time-reversed fields as it refocuses near to the source points. The explanation is that the re-compressed pulse in space and time that is statistically stable. Self-averaging in the time domain makes super-resolution is statistically stable. In the regime of high frequency, short correlations and long propagation distance, we have the statistical de-correlation of the wave functions for different frequencies

$$E \left\{ \widehat{I}(\mathbf{r}, \omega_1) \cdot \widehat{I}(\mathbf{r}, \omega_2) \right\} \approx E \left\{ \widehat{I}(\mathbf{r}, \omega_1) \right\} \cdot E \left\{ \widehat{I}(\mathbf{r}, \omega_2) \right\}, \text{ for } \omega_1 \neq \omega_2 \quad (10)$$

with $E\{\cdot\}$ being the expectation operator. Therefore,

$$\begin{aligned} E\{I(\mathbf{r}, t)^2\} &= E \left\{ \left[\int_{-\infty}^{\infty} e^{-i\omega t} \widehat{I}(\mathbf{r}, \omega) d\omega \right]^2 \right\} \\ &= E \left\{ \int_{-\infty}^{\infty} d\omega_1 \int_{-\infty}^{\infty} d\omega_2 e^{-i(\omega_1 + \omega_2)t} \widehat{I}(\mathbf{r}, \omega_1) \widehat{I}(\mathbf{r}, \omega_2) \right\} \\ &= \int_{-\infty}^{\infty} d\omega_1 \int_{-\infty}^{\infty} d\omega_2 e^{-i(\omega_1 + \omega_2)t} E \left\{ \widehat{I}(\mathbf{r}, \omega_1) \widehat{I}(\mathbf{r}, \omega_2) \right\} \quad (11) \\ &\approx \int_{-\infty}^{\infty} d\omega_1 \int_{-\infty}^{\infty} d\omega_2 e^{-i(\omega_1 + \omega_2)t} E \left\{ \widehat{I}(\mathbf{r}, \omega_1) \right\} E \left\{ \widehat{I}(\mathbf{r}, \omega_2) \right\} \\ &= E^2 \{I(\mathbf{r}, t)\} \end{aligned}$$

Using the Chebyshev's inequality, we see that for any small $\delta > 0$, the probability

$$\text{Prob}\{|I(\mathbf{r}, t) - E\{I(\mathbf{r}, t)\}| > \delta\} \leq \frac{1}{\delta^2} E\{[I(\mathbf{r}, t) - E\{I(\mathbf{r}, t)\}]^2\} \approx 0 \quad (12)$$

This means that, due to the frequency spread of the signal, I is self-averaging in the time domain, which makes super-resolution is statistically stable, that is, independent of the individual realizations of the random media.

TRM technique is widely regarded as a powerful method to image and detect targets in the complex environments. For the sake of saving space, more detailed knowledge about TRM is not mentioned here, the interested reader may consult the references [33–41]. [34, 35] give the mathematical analysis in one-dimensional or layered media and [33] for three dimensional acoustic waves in random media. [36, 37] show the self-averaging and statistical stability properties of time reversal. [38–41] report some new achievements of TRM in applications (such as application in the Microwave-Induced Thermo-Acoustic Tomography (MI-TAT) for early breast cancer detection).

3. TRM TECHNIQUE IN TWRI

Some electromagnetic requirements for UWB-TWR have been investigated in [1, 2]. A practical operational frequency is suggested about 1–3 GHz. Experimental measurements show that the complex TWR environment can result in considerable attenuation of electromagnetic waves, further more cause a complicated processing of received signals because of the multipath propagations. TRM technique has been introduced to TWRI in [29]. Below, some further work concerning more actual environments is studied. The FDTD algorithm is employed here for the simulation. Some numerical tests for 2-D electromagnetic time reversal imaging have been demonstrated.

3.1. Description of the Model

As UWB radar has much wider bandwidth than convention narrow-band radar, it is believed to have great potential in high resolution imaging. Here we assume the TWRI uses UWB system. The UWB electromagnetic source is chosen as [42]

$$p(t) = \frac{j}{[j + 2\pi f(t - t_0)/4]^5} \quad (13)$$

with a center frequency $f = 2$ GHz. j is the imaginary unit. The 3 dB frequency band is from 1.4 to 3.0 GHz.

In the simulation, imaging is done under a $5 \text{ m} \times 5 \text{ m}$ square room. The geometry is depicted in Fig. 2. The length unit here is m (same as below). The center of the room is set as the origin point. A source and a linear array are located at the outer side of the left wall. Their exact positions are declared in Fig. 2's caption. The disc scatters used as targets in the simulation are of the same relative dielectric constant $\varepsilon_r = 47$ and the same radius of 10 cm. Their positions will be given in every experiment. In the FDTD algorithm, the simulation domain is discretized to a number of cells with the size of 0.00375×0.00375 , equals to about 40 cells per wavelength in free space at the center frequency of 2 GHz.

The walls are of 0.3 m thick, with rough surface and random relative dielectric constant. The mean value of the random relative dielectric constant is $\varepsilon_r = 4$. We assume the distribution for the height of the rough surface follows the following Gauss probability density function

$$p(z) = \frac{1}{h\sqrt{2\pi}} e^{-\frac{z^2}{2h^2}} \quad (14)$$

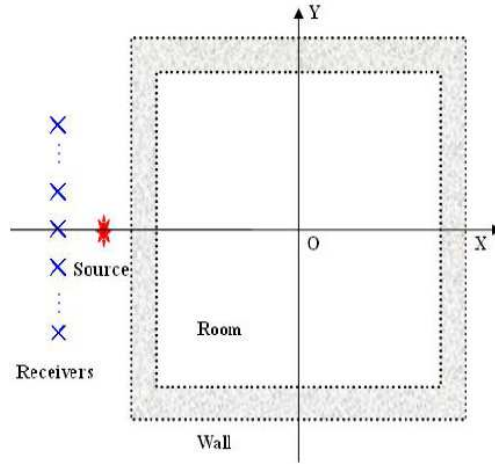


Figure 2. The sketch map of TWRI simulation settings. The dotted bounds denote rough surface. The source is positioned at the X -axis, 0.1 m away from the outer side of the left wall. The linear array with an interval of $\lambda/2$ is located symmetrically along the line $x = -2.7$.

To ensure the distribution is stable, we also introduce the following exponential function as the correlation function of the rough surface

$$R(\tau) = h^2 e^{-\tau/l} \quad (15)$$

where l is the correlation length, h is the mean square height of the rough surface. In the following simulations, we set $l = 30$, $h = 0.01$ m.

3.2. TRM Imaging under Random Walls

We firstly consider a disc scatter situated at the origin point. The homogeneous case is studied in [29]. Here we put our emphasis on the heterogeneous cases. The walls are randomized by adding their relative dielectric constant with 5 dB white Gaussian noise. Typical realization of the random wall is shown in Fig. 3. To avoid missing the multiple reflected fields, signals are recorded for a long time $T = 62.50$ ns. The linear array consists of 61 elements (receivers). In Fig. 4, the target signals from the array along time-axis are shown. We can see behind the directly reflection signals, multipath signals are significant. As to show the temporal refocusing, in Fig. 5, we plot the maximum amplitudes of the imaging domain along the time-axis. In the figure, a temporal refocusing is gained at the time $t_c = 52.32$ ns. Here $t = 0$

represents the time when signals were re-emitted from the array (the same hereinafter).

The room is selected as spatial imaging domain. Fig. 5 gives the spatial image at time t_c . We can see in the heterogeneous case the target position agrees very well with the experimental setting which means a tight spatial focusing at the target's location. The -10 dB

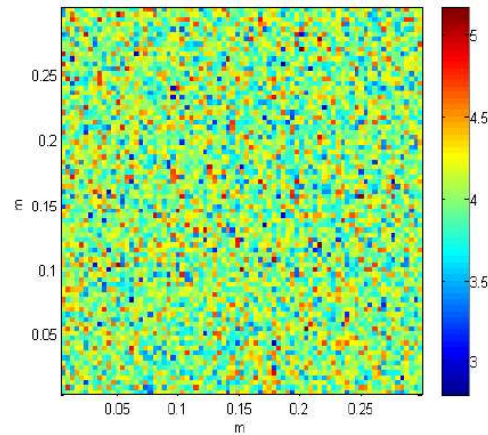


Figure 3. The typical realization of the random relative dielectric constant of a section of the walls. The mean value of the random ε_r is 4. SNR = 5 dB white Gaussian noise is added in.

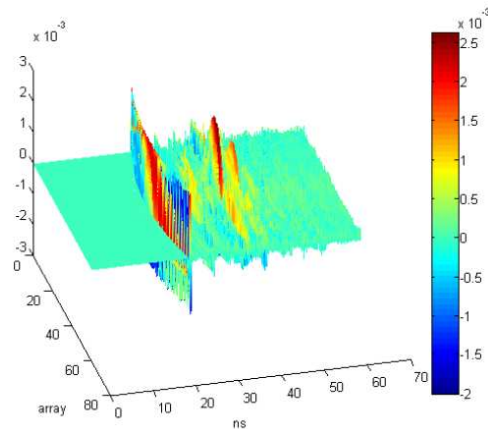


Figure 4. The target signals from the linear array. Amplitude attenuation of the recorded signals nearly reaches -52 dB.

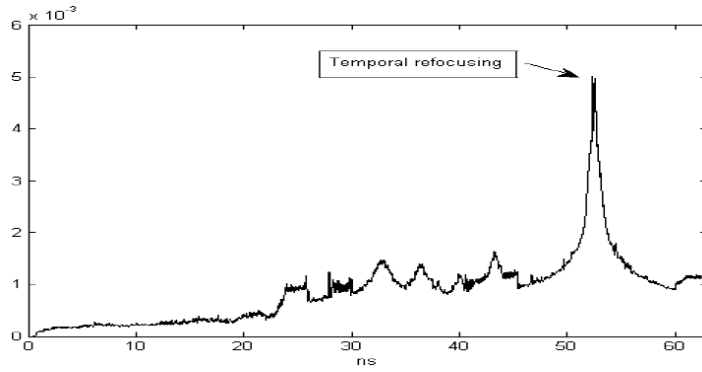


Figure 5. The maximum amplitude line of the imaging domain along the time axis. A visible temporal refocusing is gained at the time $t_c = 52.32$ ns.

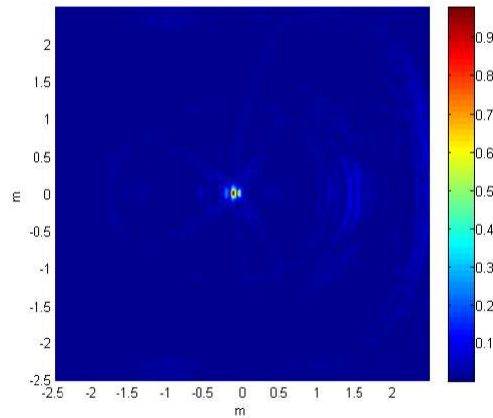


Figure 6. TRM imaging of the disc scatterer which is settled at the center of the room. The -10 dB range is 0.15 m and the ISNR is 31.60 dB.

range of the spatial focusing which approximately reflects the image resolution is 0.15 m here. Assume the imaging domain consists of I pixels. Total I_R pixels are in the -10 dB range. We defined the Imaging SNR (ISNR) as following:

$$\text{ISNR} = 10 \log \left\{ \frac{I - I_R}{I_R} \frac{\sum_{i=1}^{I_R} x_i^2}{\sum_{j=1}^{I-I_R} y_j^2} \right\} \quad (16)$$

where x_i denotes the pixels in the -10 dB range and y_j denotes the other pixels in the imaging domain.

According to Eq. (16), the ISNR for Fig. 6 is 31.60 dB. In Fig. 7, the BP method imaging result using the re-emitted signals is given as a comparison. It is clear that the focusing of TRM is much better than that of the BP method. The -10 dB range of the BP image focusing is 0.55 m, the ISNR is 27.06 dB. And it is noticed that position of the target in Fig. 7 is a little bit back of the real position. This is because the received signals are delayed in the propagation caused by the random walls but the BP imaging can not put this delay into account.

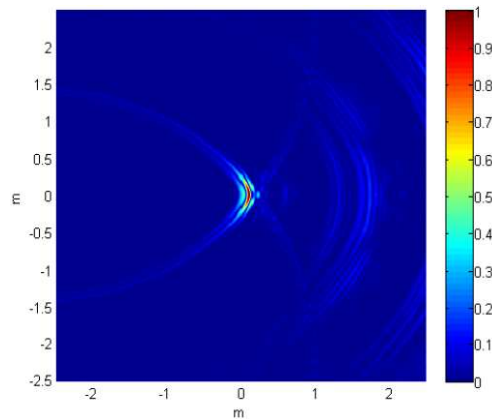


Figure 7. The BP imaging result of the disc scatterer which is settled at the center of the room. The -10 dB range is 0.55 m and the ISNR is 27.06 dB.

3.3. TRM Imaging with Contaminated Signals

The more actual situation concerning the received signals are contaminated by noises is studied in this subsection. We artificially add the recorded signals $u_T(\mathbf{r}_k, t)$ and the background signals $u_G(\mathbf{r}_k, t)$ with the white Gaussian noise. Fig. 8 is the comparison between the original signal and the contaminated signals from the 51th element of the array. As shown in Figs. 8(b) and (c), when -10 dB and -20 dB white Gaussian noises are added, the target signals are completely immersed by the noises. We re-emit the contaminated signals and investigate TRM imaging. Figs. 9(a) and (b) are the images generated by the TRM technique with -10 dB and -20 dB contaminated signals, respectively. We can see in the two figures, the target position is still

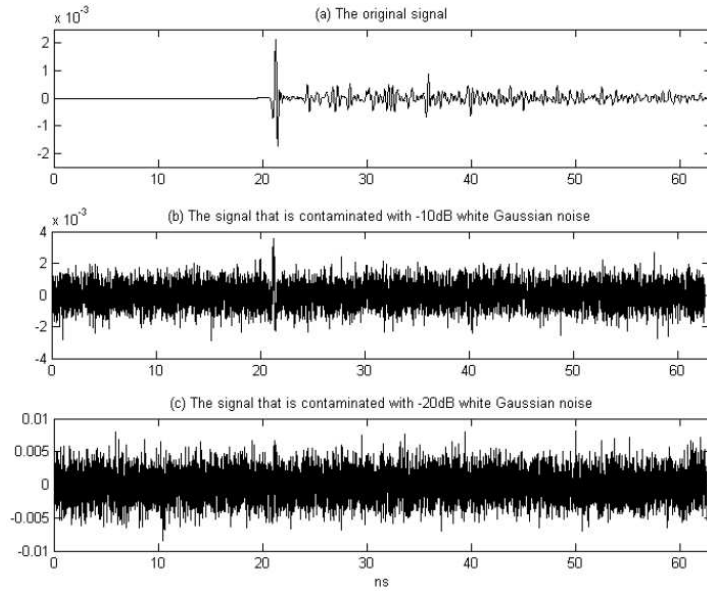


Figure 8. The original signal and the contaminated signals from the 51th element of the array.

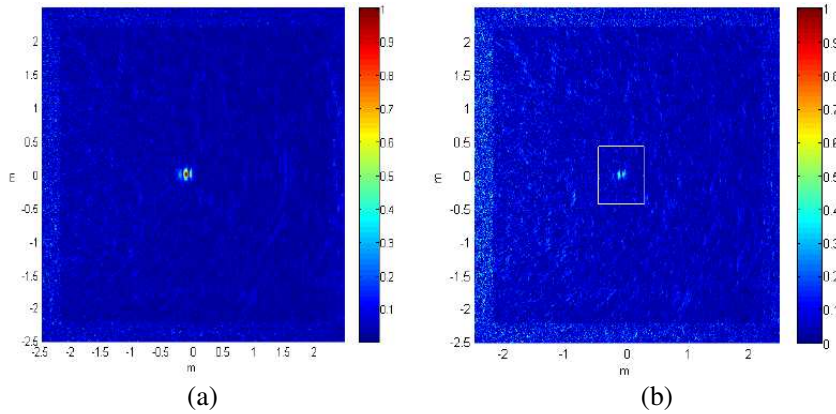


Figure 9. TRM images generate by contaminated signals. (a) is the image from -10 dB contaminated signals, and (b) is the image from -20 dB contaminated signals.

well identified. In Fig. 9(a), the -10 dB range of the image is 0.17 m and the ISNR is 28.70 dB. The corresponding values for Fig. 9(b) are 0.29 m and 20.83 dB. Figs. 10(a) and (b) are the images from BP with

-10 dB and -20 dB contaminated signals, respectively. We can see when -10 dB white Gaussian noise is added, an obscured image can be obtained. The -10 dB range of the image spread to the whole imaging domain and the -3 dB range already reaches 1.0 m. When the white Gaussian noise is increased to -20 dB, there is no visible target image from BP method.

In the random setting, based on the principle of reciprocity, TRM employs the complex environment, acts as a matched filter. Target signals follow their forward ways; arrive at the original source position in unison. Therefore, refocusing is constructive in the target position and deconstructive any where. In contrast, the noises interferes are well averaged and decreased in the processing because they are absolutely incoherent in the space and time. Hence, TRM can provide an image with higher resolution and contrast.

3.4. Evaluating the Array for TRM Imaging

In previous subsection, we all use a 5 m long array with 61 elements. This may be hard to implement in real applications. A narrow array with fewer elements will be more applicable. In this subsection, we consider the following two cases. Case 1: the linear array consists of 21 elements with an interval of $\lambda/2$. Case 2: the linear array consists of 11 elements with an interval of λ . λ is the carrier (central) wavelength of the probing pulses. In the two cases, the array is located symmetrically along the line $x = -2.7$. Fig. 11 and Fig. 12 are the TRM imaging

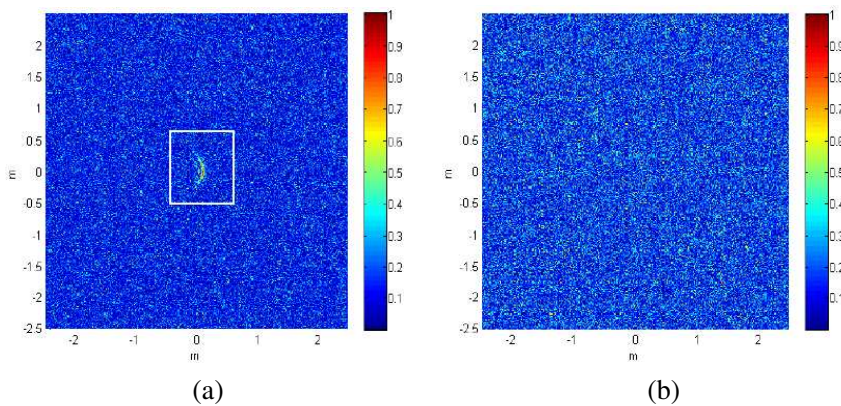


Figure 10. BP images generate by contaminated signals. (a) is the image from -10 dB contaminated signals, and (b) is the image from -20 dB contaminated signals.

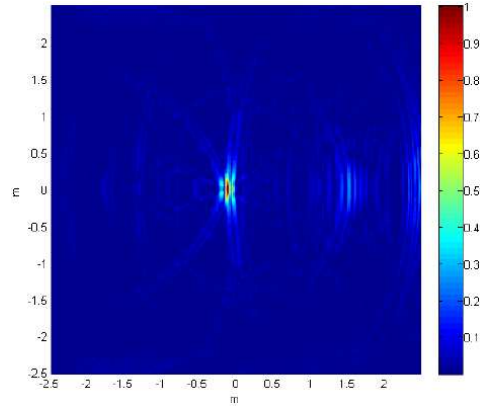


Figure 11. TRM imaging of the disc scatterer. The linear array consists of 21 elements with an interval of $\lambda/2$.

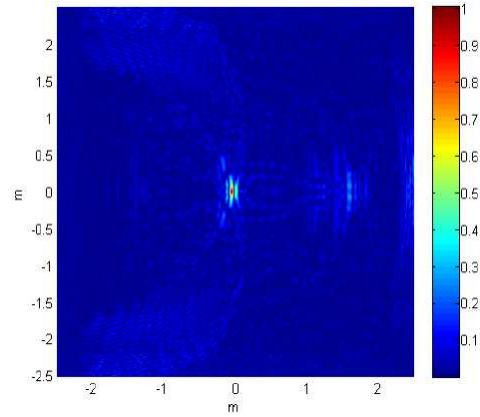


Figure 12. TRM imaging of the disc scatterer. The linear array consists of 11 elements with an interval of λ .

result for Case 1 and Case 2, respectively. The -10 dB range of the image focusing are 0.41 m for Case 1 and 0.32 cm for Case 2. The ISNR is 26.00 dB for Case 1 and 23.02 dB for Case 2. We arrive at the following statements.

1) Comparing Figs. 11, 12 with Fig. 6, we can see when the array is shorten, the resolution and the SNR of image decrease. But TRM can also give a good refocusing.

2) In [43], two adjacent elements of the linear array is suggested as $\lambda/2$ to ensure that the collection of transducers behaves like an array of

aperture $a = (K - 1)\lambda/2$ and not like separate entities, while keeping the interference between the transducers at a minimum. In Case 2, the interval is enlarged to λ . TRM give a fair image of the disc scatter. The image shows a better resolution but a lower SNR when comparing with Fig. 11.

3.5. TRM Imaging in Mismatched Environment

A more important issue about TRM in TWRI is the walls in real application are not exact known. When performing imaging, the inverse phase of TRM is done computationally, using either a measured or computed Green's function $\hat{G}_C(\mathbf{r}, \mathbf{r}_k, \omega)$ in Eq. (8). When precise knowledge of the forward environment is unavailable, we should model another related random wall to substitute it. Theoretical studies [44] illuminate that the refocusing quality of the back-propagated signals is determined by the cross-correlation of the two media. When the cross-correlation decreases, de-refocusing effects are observed. Experimental studies of electromagnetic TRM [25] demonstrated a fair refocusing at the targets location in spite of media interchanging and a substantial degradation of the TRM image as the media de-correlation increases.

To examine this issue in the TWRI, we re-use the experimental setting in Part 3.2. The re-emitted signals experience a different wall which is realized by re-adding the wall with 5 dB white Gauss noise. We investigate TRM imaging under this condition. Fig. 13 shows the imaging results. It is clear that the observations are consistent

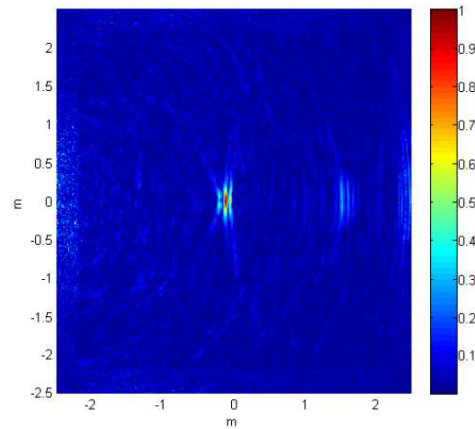


Figure 13. TRM imaging in the mismatched environment. The wall is simulated by an alone random case.

with previous studies in [25, 44]. A fair refocusing is observed at the target's location. Observation shows a reduction of the resolution and SNR when compared with the matched case (depicted in Fig. 6). The -10 dB range of the image spread to the whole imaging domain and the -3 dB range of the image is 0.25 m. The ISNR is 20.20 dB. Besides, some serious blurring is shown at the walls positions in the image. This is because the mismatched walls cause some reflections which can't be subtracted from the background signatures. They have been falsely regarded as part of target signals when performing TRM imaging.

In order to mitigate such degradation caused by environment mismatch, we may have access to the statistics of the Green's function. Specifically, assume we have obtained J realizations of the random wall, $\widehat{G}_j(\mathbf{r}, \mathbf{r}_k, \omega)$ is each corresponding Green's function, $j = 1, 2, \dots, J$. The averaged Green's function is

$$\widehat{G}_{\text{avg}}(\mathbf{r}, \mathbf{r}_k, \omega) = \frac{1}{J} \sum_{j=1}^J \widehat{G}_j(\mathbf{r}, \mathbf{r}_k, \omega) \quad (17)$$

Therefore, TRM imaging is performed by

$$\begin{aligned} \widehat{I}(\mathbf{r}, \omega) &= \sum_{k=1}^K U_B(\mathbf{r}_k, \omega) * \widehat{G}_{\text{avg}}(\mathbf{r}, \mathbf{r}_k, \omega) \\ &= \frac{1}{J} \sum_{j=1}^J \sum_{k=1}^K U_B(\mathbf{r}_k, \omega) * \widehat{G}_j(\mathbf{r}, \mathbf{r}_k, \omega) \end{aligned} \quad (18)$$

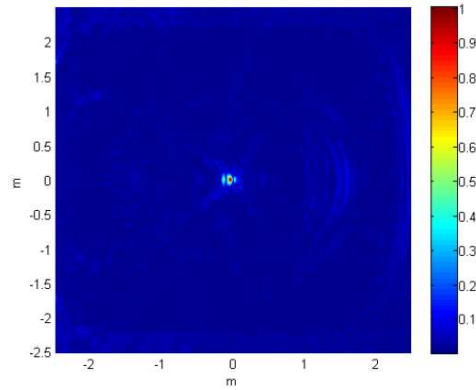


Figure 14. TRM imaging in the mismatched environment. The computational Green's function is substituted by the averaged Green's function.

We re-use the experimental data simulated in Part 3.2 and set $J = 20$, Fig. 14 is the corresponding TRM image. The -10 dB range of the image here is 0.19 m and the ISNR is 28.06 dB. Comparing with Fig. 13, application of the averaged Green's function has well improved the image quality.

4. CONCLUSIONS

TRM imaging technique has been further examined through simulation experiment for electromagnetic wave in the UWB through wall environment. Several issues of TRM in UWB-TWRI are proposed and discussed. Compared with BP method, TRM technique shows great imaging capacity in the random environment, in spite of the conditions of a narrow array or contaminated signals. In the mismatched case, observations show a degradation of the image in resolution and SNR. Application of the averaged Green's function method has well improved the image quality. However, how to employ a better Green's function in a random condition is still an interesting problem which is needed to be studied further.

ACKNOWLEDGMENT

This work is supported in part by the NSFC (No. 60771042, 60728101), 863 Program (No. 2007AA12Z159) and 08ZQ026-039 sustentation fund.

REFERENCES

1. Zhuge, X., T. G. Savalyev, and A. G. Yarovoy, "Assessment of electromagnetic requirements for UWB through-wall radar," *IEEE, Proc. ICEAA*, 923–926, 2007.
2. Yang, Y. and A. E. Fathy, "See-through-wall imaging using ultra wideband short-pulse radar system," *IEEE, Antennas and Propag. Society Inter. Symposium*, Vol. 38, 334–337, 2005.
3. Yang, Y., Y. Wang, and A. E. Fathy, "Design of compact Vivaldi antenna arrays for UWB see through wall applications," *Progress In Electromagnetics Research*, PIER 82, 401–418, 2008.
4. Hunt, A. R., "A wideband imaging radar for through-the-wall surveillance," *Proc. SPIE*, Vol. 5403, 590–596, 2004.
5. Beeri, A. and R. Daisy, "High-resolution through wall imaging," *Proc. SPIE*, Vol. 6201, 62010J, 2006.
6. Hunt, A. R., "Image formation through walls using a distributed

- radar sensor array,” *Applied Imagery Pattern Recognition Workshop*, 232–237, 2003.
7. Fan, Z. G., L. X. Ran, and J. A. Kong, “Source pulse optimizations for UWB radio systems,” *Journal of Electromagnetic Waves and Applications*, Vol. 20, 1535–1550, 2006.
 8. Zetik, R., S. Crabbe, J. Krajenak, et al., “Detection and localization of persons behind obstacles using Msequence through-the-wall radar,” *Proc. SPIE*, Vol. 6201, 62010I, 2006.
 9. Song, L.-P., C. Yu, and Q. H. Liu, “Through-wall imaging (TWI) by radar: 2-D tomographic results and analyses,” *IEEE Transactions on Geoscience and Remote Sensing*, Vol. 43, 2793–2798, 2005.
 10. Cui, G., L. Kong, and J. Yang, “A back-projection algorithm to stepped-frequency synthetic aperture through-the-wall radar imaging,” *Process of 1st Asian and Pacific Conference on Synthetic Aperture Radar*, 123–126, 2007.
 11. Abubakar, A., P. M. van den Berg, and S. Y. Semenov, “Two and three dimensional algorithms for microwave imaging and inverse scattering,” *Progress In Electromagnetics Research*, PIER 37, 57–79, 2002.
 12. Song, L. P., Q. H. Liu, F. Li, et al., “Reconstruction of three dimensional objects in layered media: Numerical experiments,” *IEEE Trans. Antennas Propagat.*, Vol. 53, 1556–1561, 2005.
 13. Ahmad, F., M. G. Amin, and G. Mandapati, “Autofocusing of through-the-wall radar imagery under unknown wall characteristics,” *IEEE Transactions on Image Processing*, Vol. 16, 1785–1795, 2007.
 14. Fink, M., “Time reversal of ultrasonic fields — Part I: Basic principles,” *IEEE Transactions on Ultrasonics, Ferroelectrics, and Frequency Control*, Vol. 39, 555–566, 1992.
 15. Fink, M., “Time reversed acoustics,” *Physics Today*, Vol. 50, 34–40, 1997.
 16. Derode, A., P. Roux, and M. Fink, “Robust acoustic time reversal with high-order multiple scattering,” *Phys. Rev. Lett.*, Vol. 75, 4206–4209, 1995.
 17. Kim, S., G. F. Edelmann, W. A. Kuperman, et al., “Spatial resolution of time-reversal arrays in shallow water,” *J. Acoust. Soc. Am.*, Vol. 110, 820–829, 2001.
 18. Borcea, L., C. Tsogka, G. Papanicolaou, et al., “Imaging and time reversal in random media,” *Inverse Problems*, Vol. 18, 1247–1279, 2002.

19. Tsogka, C. and G. Papanicolaou, "Time reversal through a solid-liquid interface and super-resolution," *Inverse Problems*, Vol. 18, 1639–1657, 2002.
20. Papanicolaou, G., L. Ryzhik, and K. Solna, "The parabolic wave approximation and time reversal," *Matematica Contemporanea*, Vol. 23, 139–160, 2002.
21. Lerosey, G., J. de Rosny, A. Tourin, et al., "Time reversal of electromagnetic waves," *Phys. Rev. Lett.*, Vol. 92, 1939041-3, 2004.
22. Liu, D., G. Kang, L. Li, et al., "Electromagnetic time-reversal imaging of a target in a cluttered environment," *IEEE Trans. Antennas Propagat.*, Vol. 53, 3058–3066, 2005.
23. Tortel, H., G. Micolau, and M. Saillard, "Decomposition of the time reversal operator for electromagnetic scattering," *Journal of Electromagnetic Waves and Applications*, Vol. 13, 687–719, 1999.
24. Liu, D., J. Krolik, and L. Carin, "Electromagnetic target detection in uncertain media: Time-reversal and minimum-variance algorithms," *IEEE Transactions on Geoscience and Remote Sensing*, Vol. 45, 934–944, 2007.
25. Liu, D., S. Vasudevan, J. Krolik, et al., "Electromagnetic time-reversal source localization in changing media: Experiment and analysis," *IEEE Trans. Antennas Propagat.*, Vol. 55, 344–354, 2007.
26. Chen, X., "Time-reversal operator for a small sphere in electromagnetic fields," *Journal of Electromagnetic Waves and Applications*, Vol. 21, 1219–1230, 2007.
27. Rao, T. and X. Chen, "Analysis of the time-reversal operator for a single cylinder under two-dimensional settings," *Journal of Electromagnetic Waves and Applications*, Vol. 20, 2153–2165, 2006.
28. Chambers, D. H. and J. G. Berryman, "Analysis of the time-reversal operator for a small spherical scatterer in an electromagnetic field," *IEEE Trans. Antennas Propagat.*, Vol. 52, 1729–1738, 2004.
29. Zheng, W., Z. Zhao, and Z. Nie, "Application of TRM in the UWB through wall radar," *Progress In Electromagnetics Research*, PIER 87, 279–296, 2008.
30. Born, M. and E. Wolf, *Principles of Optics*, Academic Press, New York, 1970.
31. Blomgren, P., G. Papanicolaou, and H. Zhao, "Super-resolution in time-reversal acoustics," *J. Acoust. Soc. Am.*, Vol. 111, 230–248,

- 2002.
32. Kuperman, W. A., W. S. Hodgkiss, H. C. Song, et al., "Phase conjugation in the ocean: Experimental demonstration of an acoustic time reversal mirror," *J. Acoust. Soc. Am.*, Vol. 103, 25–40, 1998.
 33. Bal, G. and L. Ryzhik, "Time reversal and refocusing in random media," *SIAM J. on Appl. Math.*, Vol. 63, 1475–1498, 2003.
 34. Clouet, J. F. and J.-P. Fouque, "A time-reversal method for an acoustical pulse propagating in randomly layered media," *Wave Motion.*, Vol. 25, 361–368, 1997.
 35. Fouque, J.-P. and K. Solna, "Time reversal aperture enhancement," *SIAM Mult. Mod. Simul.*, Vol. 1, 239–259, 2003.
 36. Bal, G., G. Papanicolaou, and L. Ryzhik, "Self-averaging in time reversal for the parabolic wave equation," *Stochastics and Dynamics*, Vol. 2, 507–531, 2002.
 37. Papanicolaou, G., L. Ryzhik, and K. Solna, "Statistical stability in time reversal," *SIAM J. on Appl. Math.*, Vol. 64, 1133–1155, 2004.
 38. Chen, G. P., W. B. Yu, Z. Q. Zhao, et al., "The prototype of microwave-induced thermo-acoustic tomography imaging by time reversal mirror," *Journal of Electromagnetic Waves and Applications*, Vol. 22, 1565–1574, 2008.
 39. Chen, G. P., Z. Q. Zhao, and Q. H. Liu, "Computational study of time reversal mirror technique for microwave-induced thermo-acoustic tomography," *Journal of Electromagnetic Waves and Applications*, Vol. 22, 2191–2204, 2008.
 40. Xiao, S. Q., J. Chen, B.-Z. Wang, et al., "A numerical study on time-reversal electromagnetic wave for indoor ultra-wideband signal transmission," *Progress In Electromagnetics Research*, PIER 77, 329–342, 2007.
 41. Liu, X., B.-Z. Wang, S. Xiao, et al., "Performance of impulse radio UWB communications based on time reversal technique," *Progress In Electromagnetics Research*, PIER 79, 401–413, 2008.
 42. Zhao, Z., N. Li, J. Smith, et al., "Analysis of scattering from very large three-dimensional rough surface using MLFMM and ray-based analyses," *IEEE Antennas and Propagation Magazine*, Vol. 47, 20–30, 2005.
 43. Steinberg, B., *Microwave Imaging with Large Antenna Arrays*, Wiley, New York, 1983.
 44. Bal, G. and R. Verastegui, "Time reversal in changing environment," *Multiscale Model. Simul.*, Vol. 2, 639–661, 2004.